Theoretical calculations of core-core-valence Auger spectra: Applications to the $L_3M_{2,3}V$ transitions of Ti in nonstoichiometric Ti-C, Ti-N, and Ti-O

G. Hörmandinger, P. Weinberger, P. Marksteiner,* and J. Redinger
Institut für Technische Elektrochemie, Technische Universität Wien, Getreidemarkt 9/158, A-1060 Wien, Austria
(Received 10 December 1987)

A formalism is derived to calculate the intensities of core-core-valence Auger spectra using results of band-structure calculations. The spectra obtained can be interpreted in terms of local partial densities of states. This method is applied to the $L_3M_{2,3}V$ transitions of Ti in the systems Ti-C, Ti-N, and Ti-O for ordered and disordered structures. In the case of Ti-C and Ti-O, a comparison with experimental spectra shows good agreement, especially concerning the influence of nonstoichiometry on the line shapes of the spectra.

I. INTRODUCTION

For quite a few years Auger electron spectroscopy (AES) has been a standard technique for the chemical analysis of solids by using the energetical positions of peaks to identify the elements in a specimen and by using the relative peak intensities to determine the chemical composition. Auger spectra of solids provide, however, much more information, in particular with respect to peak shapes of valence-band electrons: Rather than using them only as "fingerprints," theoretical spectra can be calculated in order to interpret the line shapes of the experimental spectra.

Among the two types of Auger processes mapping the valence band, namely the core-core-valence (CCV) AES and the core-valence-valence (CVV) AES, obviously the former is more suitable for a comparison between theory and experiment, because in the latter case a kind of self-folding of the density of states (DOS) is involved and therefore in this case interpretation of experimental data is much more difficult. Since the two core holes in a CCV process are localized at one atomic site, the peak shape is determined by the local partial DOS (PDOS). The CCV spectrum, however, is not just the PDOS, corrected for lifetime broadening and spectrometer resolution, but symmetry-dependent matrix elements occur which can differ considerably for the various angular-momentum-dependent channels.

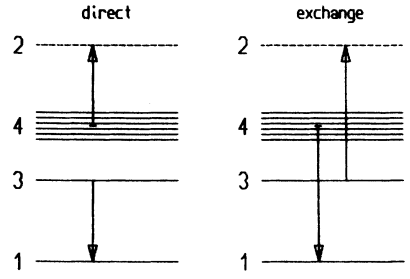

FIG. 1. Energy-level scheme for a core-core-valence Auger process. Arrows show electron transitions (left, for the direct; right, for the exchange matrix elements). The numbering refers to hole states: 1,2 before, 3,4 after the Auger transition, respectively.

In Sec. II of the present work a spectral representation of the valence-band Green's function is used to introduce the DOS into the expression for the Auger transition probability. Together with the DOS the matrix elements obtained yield the intensity for CCV spectra.

Applications of this method to the technologically important systems Ti-C, Ti-N, and Ti-O are shown in Sec. III. Various concentrations of vacancies on the nonmetal sublattices are considered and the peak shapes are found to be strongly dependent on these concentrations. Experimental results show good agreement with the calculations.

II. THEORY

A. Auger transitions in solids

Within a nonrelativistic treatment of the Auger process the transition probability P is given by the well-known formula (see, e.g., Chattarji[1]):

$$P=\frac{2\pi}{\hbar}\,|D-E|^2\delta(\varepsilon_3-\varepsilon_1+\varepsilon_4-\varepsilon_2)\,, \tag{2.1}$$

where the matrix elements D and E are of the form

$$D=\int\int\psi_1^*(\mathbf{r}_1)\psi_2^*(\mathbf{r}_2)\frac{e^2}{|\mathbf{r}_1-\mathbf{r}_2|}\psi_3(\mathbf{r}_1)\psi_4(\mathbf{r}_2)d^3r_1d^3r_2\,,$$
$$E=\int\int\psi_1^*(\mathbf{r}_1)\psi_2^*(\mathbf{r}_2)\frac{e^2}{|\mathbf{r}_1-\mathbf{r}_2|}\psi_4(\mathbf{r}_1)\psi_3(\mathbf{r}_2)d^3r_1d^3r_2\,. \tag{2.2}$$

In the case of CCV transitions, indices 1 and 3 denote wave functions (WF's) of the core states, 2 is the continuum WF of the outgoing electron, and the information concerning the valence band is contained in the functions $\psi_4(\mathbf{r})$ (see Fig. 1). Since we are not interested in absolute Auger yields, we shall omit the factor $2\pi/\hbar$ in the following. In order to introduce the Green's function associated with the valence WF's we consider the square of (2.1) explicitly:

$$|D-E|^2=|D|^2+|E|^2-2\,\mathrm{Re}(D^*E)\,. \tag{2.3}$$

Let us consider the $|D|^2$ term first. The magnetic quantum numbers of the core states 1 and 3 are inobservables and therefore can be summed up. Also, a sum over all valence states with energies ε_4 has to be performed:

$$\overline{|D(\varepsilon_2)|^2}=\sum_{m_1,m_3}\sum_{\substack{\text{all}\\ \text{valence}\\ \text{states}}}|D(\varepsilon_4)|^2\delta(\varepsilon_3-\varepsilon_1+\varepsilon_4-\varepsilon_2)$$

$$=\int d\varepsilon\sum_{m_1,m_3}\sum_{\substack{\text{all}\\ \text{valence}\\ \text{states}}}|D(\varepsilon_4)|^2\delta(\varepsilon_3-\varepsilon_1+\varepsilon-\varepsilon_2)\delta(\varepsilon-\varepsilon_4)\ . \tag{2.4}$$

The expression on the right-hand side of (2.4) contains a sum of the form

$$\sum_{\substack{\text{all}\\ \text{valence}\\ \text{states}}}\psi_4^*(\mathbf{r}_2,\varepsilon_4)\psi_4(\mathbf{r}_2',\varepsilon_4)\delta(\varepsilon-\varepsilon_4)$$

$$=-\frac{1}{\pi}\mathrm{Im}G(\mathbf{r}_2,\mathbf{r}_2',\varepsilon),\quad L=(l,m)\ . \tag{2.5}$$

Energy conservation is provided by the delta function $\delta(\varepsilon_3-\varepsilon_1+\varepsilon-\varepsilon_2)$. Performing the energy integral in (2.4), ε_2 equals $\varepsilon+\varepsilon_3-\varepsilon_1$. Equation (2.4) can therefore be written as a function of ε. According to Faulkner and Stocks,[2] the Green's function $G(\mathbf{r},\mathbf{r}',\varepsilon)$ is given in terms of the site-diagonal scattering path operator $\tau^{nn}(\varepsilon)$ by

$$\mathrm{Im}G(\mathbf{r},\mathbf{r}',\varepsilon)=\sum_{L,L'}Z_L^n(\mathbf{r},\varepsilon)\mathrm{Im}\tau_{LL'}^{nn}(\varepsilon)Z_{L'}^n(\mathbf{r}',\varepsilon)\ , \tag{2.6}$$

where the functions $Z_L^n(\mathbf{r},\varepsilon)$ are regular solutions of the Schrödinger equation for the nth central field and are normalized to single-site scattering. In the case of the Auger process, $\mathbf{r}$ and $\mathbf{r}'$ lie in the same sphere and therefore the index n will be dropped in the following.

Using (2.6), instead of the valence WF's $\psi_4(\mathbf{r},\varepsilon_4)$ the functions $Z_L(\mathbf{r},\varepsilon)$ occur in $|D|^2$. For the core states, atomic WF's are used:

$$\psi_j(\mathbf{r},\varepsilon_j)=R_{l_j}(r,\varepsilon_j)Y_{L_j}(\Omega)\ , \tag{2.7}$$

with $j=1$ or 3. The outgoing Auger electron is described by a time-reversed LEED state, the details of which are given elsewhere (see Redinger, Marksteiner, and Weinberger[3] and references therein). Assuming that the electron is not scattered any further on its way out (the so-called single-scatterer final-state approximation) this state is given by

$$\psi_2(\mathbf{r},\varepsilon_2)=4\pi\sum_{L_2}i^{l_2}Y_{L_2}^*(\Omega_k)e^{i\delta_{l_2}(\varepsilon_2)}\tilde{Z}_{l_2}(r,\varepsilon_2)Y_{L_2}(\Omega)\ . \tag{2.8}$$

The functions $\tilde{Z}_l(r,\varepsilon)$ are regular solutions of the Schrödinger equation normalized to Bessel and Neumann functions at the muffin-tin radius. Ω_k is the angle of the wave vector $\mathbf{k}$ which is antiparallel to the direction of the outgoing electron. Using the identity

$$\frac{1}{|\mathbf{r}_1-\mathbf{r}_2|}=\sum_{\Lambda}\gamma_\lambda(r_1,r_2)Y_\Lambda(\Omega_1)Y_\Lambda^*(\Omega_2)\ , \tag{2.9}$$

where Λ denotes (λ,μ) and

$$\gamma_\lambda(r_1,r_2)=\frac{r_<^\lambda}{r_>^{\lambda+1}}\ , \tag{2.10}$$

we can now write the complete expression for the D^2 term as follows:

$$\overline{|D(\varepsilon)|^2}=-\frac{1}{\pi}(4\pi)^2\sum_{L,L'}\sum_{m_1,m_3}\Bigg[\int\int d^3r_1d^3r_2R_{l_1}^*(r_1,\varepsilon_1)Y_{l_1}^*(\Omega_1)$$
$$\times\sum_{L_2}(-i)^{l_2}Y_{L_2}(\Omega_k)e^{-i\delta_{l_2}(\varepsilon_2)}\tilde{Z}_{l_2}^*(r_2,\varepsilon_2)Y_{L_2}^*(\Omega_2)$$
$$\times\sum_{\Lambda}\gamma_\lambda(r_1,r_2)Y_\Lambda^*(\Omega_1)Y_\Lambda(\Omega_2)R_{l_3}(r_1,\varepsilon_3)Y_{L_3}(\Omega_1)Z_l(r_2,\varepsilon)Y_L(\Omega_2)\Bigg]$$
$$\times\mathrm{Im}\tau_{LL'}(\varepsilon)+[\text{c.c.}]\ . \tag{2.11}$$

Angular integration over Ω_k diagonalizes (2.11) with respect to L_2 and L_2', whereby L_2' refers to the complex-conjugate part in (2.11). The angular part of (2.11) consists of four integrals of the form

$$\int d\Omega\,Y_{L_1}(\Omega)Y_{L_2}(\Omega)Y_{L_3}(\Omega)=\left[\frac{1}{4\pi}(2l_1+1)(2l_2+1)(2l_3+1)\right]^{1/2}\begin{pmatrix}l_1 & l_2 & l_3\\ 0 & 0 & 0\end{pmatrix}\begin{pmatrix}l_1 & l_2 & l_3\\ m_1 & m_2 & m_3\end{pmatrix}, \tag{2.12}$$

where the

$$\begin{pmatrix}l_1 & l_2 & l_3\\ m_1 & m_2 & m_3\end{pmatrix}$$

are Wigner $3j$ symbols. In order to replace $\mathrm{Im}\tau_{LL'}(\varepsilon)$ in the expression for the transition probability by the partial DOS

$n_l(\varepsilon)$, we use the following approximation:

$$\mathrm{Im}\tau_{LL'}(\varepsilon)\cong\frac{-\pi}{2l+1}n_l(\varepsilon)F^{-1}_{LL'}(\varepsilon)\delta_{LL'}\ , \tag{2.13}$$

where $F_{LL'}(\varepsilon)$ is given by

$$F_{LL'}(\varepsilon)=\int_{\Omega_{\mathrm{WS}}}d^3r\,Z_L(\mathbf{r},\varepsilon)Z_{L'}(\mathbf{r},\varepsilon) \tag{2.14}$$

and Ω_{WS} is the volume of the Wigner-Seitz sphere. Using the orthogonality relation for $3j$ symbols and defining the integrals

$$I^{\lambda}(f_1,f_2\,|\,f_3,f_4)=\int\int r_1^2\,dr_1r_2^2\,dr_2f_1^*(r_1)f_2^*(r_2)\gamma_{\lambda}(r_1,r_2)f_3(r_1)f_4(r_2)\ , \tag{2.15}$$

$$F_l(\varepsilon)=F_{LL'}(\varepsilon)\delta_{ll'}\delta_{mm'}\ , \tag{2.15a}$$

we finally get the following expression for the D^2 term:

$$\overline{|D(\varepsilon)|^2}=\sum_l\sum_{\lambda}\sum_{l_2}(2l_1+1)(2l_3+1)(2\lambda+1)(2l_2+1)\begin{pmatrix}l_1&\lambda&l_3\\0&0&0\end{pmatrix}^2\begin{pmatrix}l&\lambda&l_2\\0&0&0\end{pmatrix}^2$$

$$\times|I^{\lambda}(R_{l_1}(\varepsilon_1)\tilde{Z}_{l_2}(\varepsilon_2)\,|\,R_{l_3}(\varepsilon_3)Z_l(\varepsilon))|^2F_l^{-1}(\varepsilon)n_l(\varepsilon)\ . \tag{2.16}$$

The same procedure can be applied to the $|E|^2$ term in Eq. (2.3):

$$\overline{|E(\varepsilon)|^2}=\sum_l\sum_{\lambda}\sum_{l_2}(2l_1+1)(2l_3+1)(2\lambda+1)(2l_2+1)\begin{pmatrix}l_1&\lambda&l\\0&0&0\end{pmatrix}^2\begin{pmatrix}l_3&\lambda&l_2\\0&0&0\end{pmatrix}^2$$

$$\times|I^{\lambda}(R_{l_1}(\varepsilon_1)\tilde{Z}_{l_2}(\varepsilon_2)\,|\,Z_l(\varepsilon)R_{l_3}(\varepsilon_3))|^2F_l^{-1}(\varepsilon)n_l(\varepsilon)\ . \tag{2.17}$$

Note that as compared with the integral in $|D|^2$ the functions $R_{l_3}(r,\varepsilon_3)$ and $Z_l(r,\varepsilon)$ in I^{λ} occur in reverse order. The cross term D^*E is less compact:

$$\overline{D^*E(\varepsilon)}=\sum_l\sum_{\lambda}\sum_{\lambda'}\sum_{l_2}(2l_1+1)(2l_3+1)(2\lambda+1)(2\lambda'+1)(2l_2+1)(-1)^{l_3+\lambda'+l_1}$$

$$\times\begin{pmatrix}l_1&\lambda&l_3\\0&0&0\end{pmatrix}\begin{pmatrix}l&\lambda&l_2\\0&0&0\end{pmatrix}\begin{pmatrix}l_1&\lambda'&l\\0&0&0\end{pmatrix}\begin{pmatrix}l_3&\lambda'&l_2\\0&0&0\end{pmatrix}\begin{Bmatrix}l_3&\lambda'&l_2\\l&\lambda&l_1\end{Bmatrix}$$

$$\times[I^{\lambda}(R_{l_1}(\varepsilon_1)\tilde{Z}_{l_2}(\varepsilon_2)\,|\,R_{l_3}(\varepsilon_3)Z_l(\varepsilon))]^*[I^{\lambda}(R_{l_1}(\varepsilon_1)\tilde{Z}_{l_2}(\varepsilon_2)\,|\,Z_l(\varepsilon)R_{l_3}(\varepsilon_3))]F_l^{-1}(\varepsilon)n_l(\varepsilon)\ . \tag{2.18}$$

In (2.18),

$$\begin{Bmatrix}l_3&\lambda'&l_2\\l&\lambda&l_1\end{Bmatrix}$$

is a $6j$ symbol. Using (2.16)–(2.18), we can define factors $\sigma_l(\varepsilon)$ such that the transition rate for a CCV Auger transition assumes the form

$$P(\varepsilon)=\sum_l\sigma_l(\varepsilon)n_l(\varepsilon)\ . \tag{2.19}$$

The σ_l are matrix elements and act as weighting factors for the l-dependent local PDOS. Since they can be very different in magnitude, the shape of the Auger spectrum can deviate considerably from that of the total PDOS at an atomic site.

B. Approximations and restrictions of the method

Due to the approximations used in the derivation of Eqs. (2.16)–(2.18), calculations of Auger spectra as described above are not generally valid. The main effect omitted is the interaction of the two holes left on the atomic site so that we are restricted to cases where this kind of interaction is small enough to be neglected. This is the case, e.g., for the early $3d$ metals. With increasing atomic number in the $3d$ row the hole-hole interaction energy grows as compared with the width of the valence band and becomes dominant in the vicinity of Ni (see, e.g., Antonides, Janse, and Sawatzky[4]). This interaction leads to quasiatomic Auger spectra for the $3d$ elements with higher atomic number than Ni (Sawatzky,[5] Sawatzky and Lenselink[6]). In the case of Ti, however,

our method should be applicable and in fact correspondence between theory and experiment is quite satisfactory as will be shown in Sec. III.

Another restriction arises from the fact that the calculation is nonrelativistic so that heavy elements cannot be treated and that the spin is not taken into account. Since spin-orbit coupling is non-negligible even for the lighter elements, we consider this effect in an approximate manner by assuming that the contribution of a special energy level to the spectrum depends linearly on its occupation. In the case of the $L_3M_{2,3}V$ transition this means that the total spectrum consists of a superposition of two identical L_3M_3V-type spectra, shifted apart on the energy scale and weighted by the proper degeneracy of the core levels. The energy shift, that is, the LS splitting between M_2 and M_3, is obtained from atomic calculations.

Although AES is a surface sensitive technique, we use a bulk formalism. The mean free path of the Auger electrons is of the order of about 10 Å (see the standard formulas of Seah and Dench[7] or Tokutaka, Nishimori, and Hayashi;[8] for rutile, Duc *et al.*[9] report a mean free path of 18 Å for the 387-eV Auger electrons). Surface effects will therefore be important.

Apart from these restrictions, our theoretical spectra are subject to several calculational simplifications, e.g., the assumption that the outgoing Auger electrons undergo no further scattering. Furthermore, an approximation for the scattering-path operator in terms of the local densities of states is used. This last approximation is formally not necessary but it greatly simplifies the interpretation of experimental spectra in terms of PDOS.

III. RESULTS AND DISCUSSION

The self-consistent APW potentials used in the present calculations were, in the case of Ti-C and Ti-N, taken from Neckel *et al.*,[10] for the construction of the vacancy potentials see in detail Marksteiner *et al.*[11] The Ti-O APW potential originates from Herzig.[12] The local partial densities of states for Ti-C and Ti-N were taken from Marksteiner *et al.*,[11] the PDOS of ordered Ti-O was provided by Herzig.[12] The CPA DOS of partially disordered Ti-O was calculated by Marksteiner, Hörmandinger, and Weinberger.[13]

The matrix elements for Ti LMV transitions corresponding to (2.19) are shown in Fig. 2 for the systems Ti-$C_{1.0}$, Ti-$N_{1.0}$, and Ti-$O_{1.0}$. In all three cases the d-type states (t_{2g},e_g) take part in the Auger process much more than s- (a_{1g}) or p- (t_{1u}) type states. Since t_{2g} and e_g contributions are dominant in the local PDOS at the Ti site, the spectra map almost exclusively the d-type local PDOS. There are only small differences between the matrix elements of Ti in the considered systems which, however, were to be expected because a different atomic environment enters the expression for the matrix elements only via the muffin-tin potential, that is, via the functions Z_l and $\tilde{Z}_l$. Changes in the environment affect mainly the outer zone of a muffin-tin sphere while the dominant contributions to the integrals in (2.15) come from a radial regime close to the center where the core functions R_l are large. Differences between matrix elements for the same

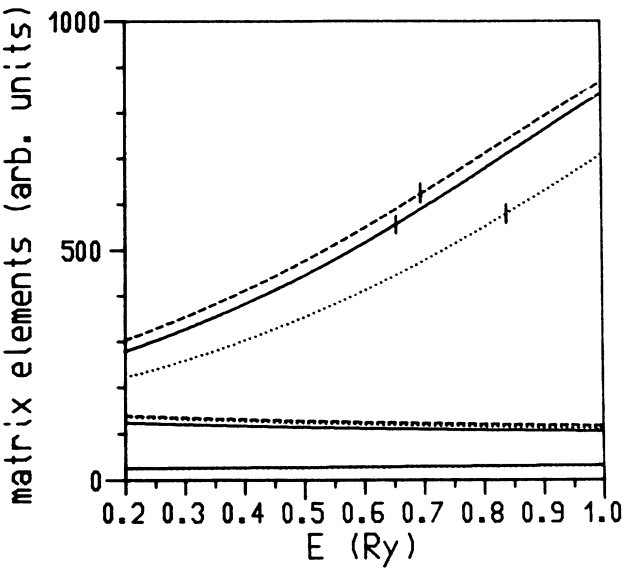

FIG. 2. Comparison of matrix elements for $TiC_{1.0}$, $TiN_{1.0}$, and $TiO_{1.0}$ (the latter with 15% vacancies on each sublattice). Solid lines, Ti-C; dotted, Ti-N; dashed, Ti-O. The energy scale refers to the muffin-tin potential with interstitial regions at zero potential. The Fermi energy of each system is marked in the d-type curves (0.66, 0.842, and 0.7 Ry for $TiC_{1.0}$, $TiN_{1.0}$, and $TiO_{1.0}$, respectively).

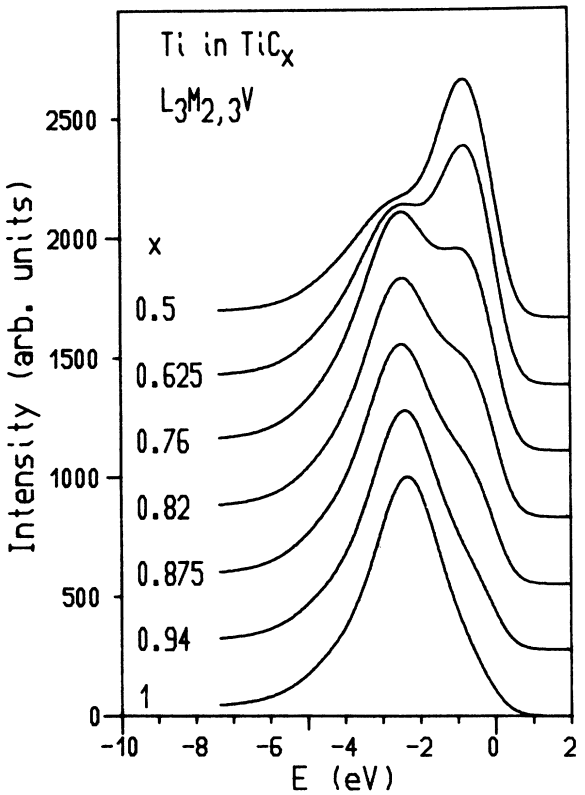

FIG. 3. $L_3M_{2,3}V$ Auger spectra for Ti in TiC_x with x varying between 0.5 and 1. The spectrometer resolution is taken to be 1 eV FWHM. The spectra consist of two contributions shifted relatively in energy (see Fig. 4 and Sec. II B) and are normalized to the same maximum value. The zero of the energy scale is the Fermi energy of the upper contribution.

system but different compositions are even smaller. The energy scale in Fig. 2 refers to the muffin-tin potential used for the calculation of the DOS, where the constant potential between the muffin tins is zero.

As has been described above, *L-S* coupling has been taken into account by superposing the single spectra on an energy scale shifted according to the *L-S* energy splits of the core levels. For the transition *LMV* this would lead to a superposition of the L_2M_2V, L_2M_3V, L_3M_2V, and L_3M_3V spectra. However, it is a well-known fact that experimentally only the $L_3M_{2,3}V$ contribution is observed in Ti due to Coster-Kronig processes in the *L* shell (see, e.g., Duc *et al.*[9] and references therein or de Boer[14]). For that reason, superposition of single spectra was carried out only with respect to the $M_{2,3}$ levels where the energy shift was taken to be 0.71 eV. As can be seen in Figs. 4, 8, and 9 the general form of the spectrum is not very much affected by this procedure.

Auger $L_3M_{2,3}V$ spectra of TiC_x are shown in Fig. 3 with compositions varying between $x=0.5$ and $x=1$. In the case of the stoichiometric composition there exists a single peak with approximately equal t_{2g} and e_g contributions (Fig. 4, bottom right). With decreasing carbon content a second peak arises about 1.6 eV higher in energy, consisting of a mainly t_{2g} and a smaller e_g contribution (Fig. 4, top right). The latter peak becomes dominant for x less than 0.7. This behavior is caused by the form of the local PDOS (see Marksteiner *et al.*[11]): Both the t_{2g} and e_g contribution roughly consist of two bands, the upper bands lying above the Fermi energy (E_F) for the stoichiometric composition. As x decreases, they are shifted to lower energies and the portion below E_F appears in the spectrum. The lower bands maintain their energies but are reduced in magnitude. Comparison with experimental spectra taken from Gutsev and Shul'ga[15] shows good agreement as far as the tendency from the lower to the higher peak is concerned (Fig. 5). However,

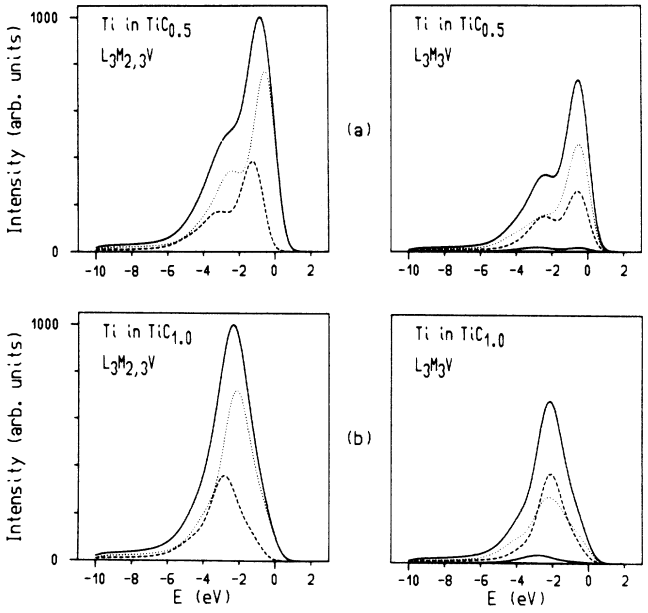

FIG. 4. Left: decomposition of the Ti $L_3M_{2,3}V$ spectrum in (a) $TiC_{0.5}$ and (b) $TiC_{1.0}$ into its L_3M_2V (at lower energy) and L_3M_3V contributions. Right: further decomposition of the L_3M_3V part into partial *l*-like spectra. Top solid line, total; dotted, t_{2g}; dashed, e_g; bottom solid curve, *p* contribution. The *s*-like contribution is too small to be shown on this scale.

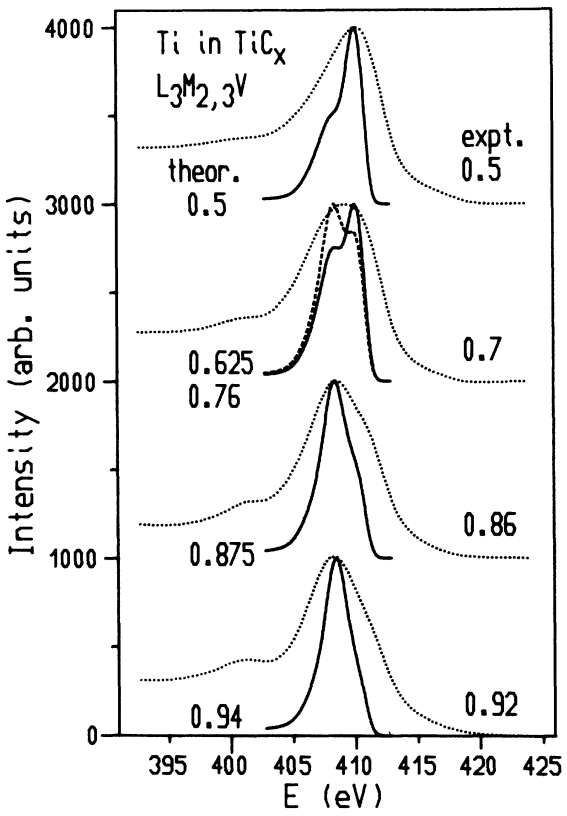

FIG. 5. Comparison of theoretical (solid lines) and experimental (dotted lines) Ti $L_3M_{2,3}V$ spectra in Ti-C for various concentrations of carbon. The dashed curve is $TiC_{0.76}$, the solid curve at the same position is $TiC_{0.625}$. Experimental results are taken from Gutsev and Shul'ga (Ref. 15). The theoretical spectra are shifted in energy to fit the experiment (whereby energy shifts are equal for all cases).

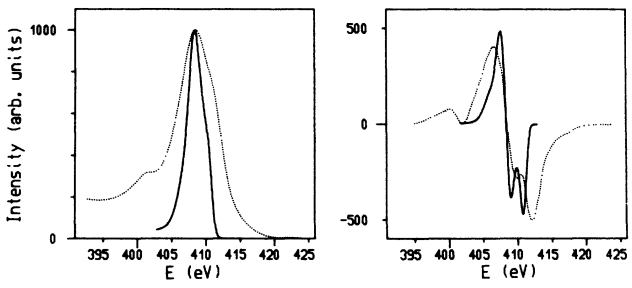

FIG. 6. Inherent difficulties in comparing theoretical with experimental AES spectra are shown for the case of $TiC_{0.875}$ (theoretical) and $TiC_{0.86}$ (experimental), respectively. Left, Auger spectra $N(E)$; right, derivative $N'(E)$ with respect to the energy. The experimental curves are taken from Gutsev and Shul'ga (Ref. 15).

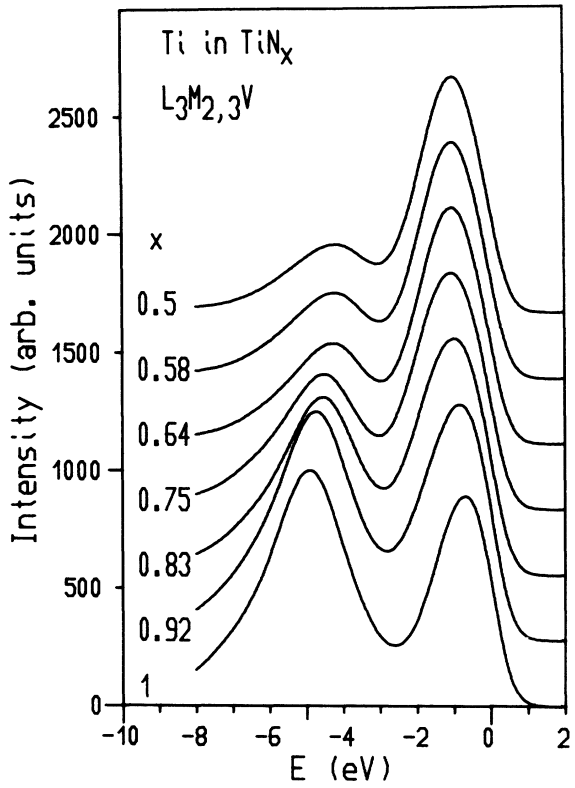

FIG. 7. $L_3M_{2,3}V$ Auger spectra for Ti in TiN_x with x varying between 0.5 and 1. The spectrometer resolution is 1 eV FWHM.

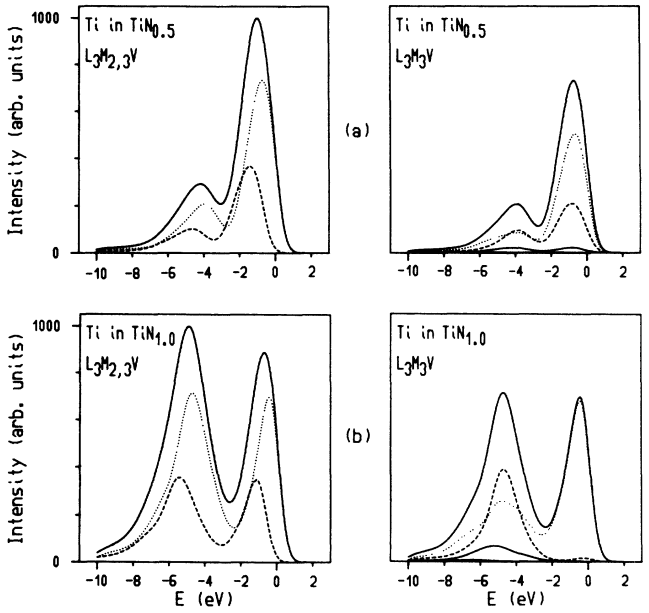

FIG. 8. Left: decomposition of the Ti $L_3M_{2,3}V$ spectrum in (a) $TiN_{0.5}$ and (b) $TiN_{1.0}$ into its L_3M_2V (at lower energy) and L_3M_3V contributions. Right: further decomposition of the L_3M_3V part into partial l-like spectra. Top solid line, total; dotted, t_{2g}; dashed, e_g; bottom solid curves, s and p contributions. The s-like contribution is nearly invisible.

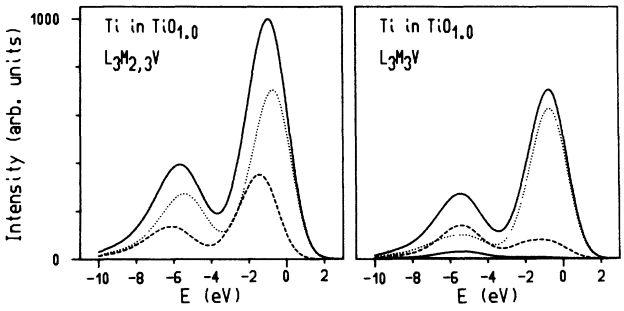

FIG. 9. $L_3M_{2,3}V$ spectrum of Ti in $TiO_{1.0}$ with 15% vacancies on both sublattices. The spectrometer resolution is 1.8 eV FWHM. Decomposition of the spectrum analogous to Figs. 4 and 8.

their curves are much broader than ours. The small peak at the low-energy side of the experimental spectra most probably arises from hybridizations of Ti p-like states to the nonmetal s band (see, e.g., Neckel *et al.*[10]) the energy regime of which was not taken into account in the present calculation.

As far as a comparison of calculated and experimental spectra is concerned, one has to decide whether to compare the spectra themselves or their derivatives with respect to the energy. Generally experimental data are published as first derivative $N'(E)$ of the spectrum $N(E)$. It seems therefore reasonable to calculate the theoretical $N'(E)$ and look for similarities. However, the right-hand part of Fig. 6 shows that this attempt leads to quite frustrating results. Especially the energetical positions of the "peaks," the points of inflection of the spectra, are rather different due to the stronger broadening of the experi-

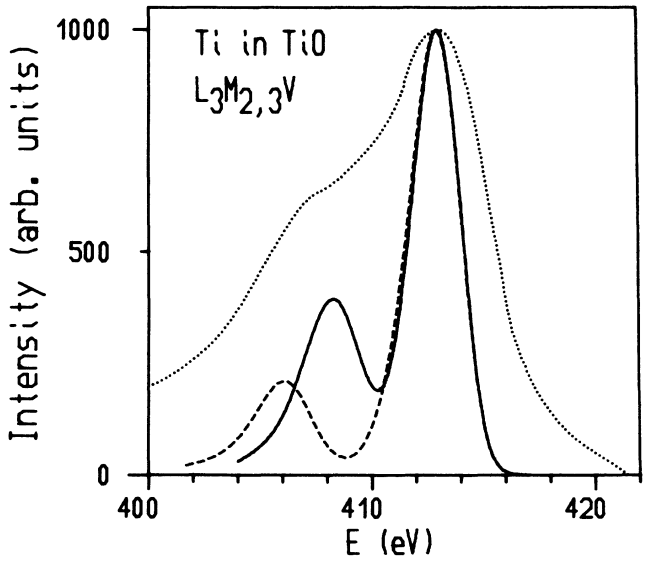

FIG. 10. Comparison of theoretical and experimental results for Ti-O. Solid line, 15% vacancies on both sublattices: dashed line, ordered Ti-O. Dotted curve: experimental results as taken from Solomon and Baun (Ref. 16).

mental curves. In the case of "integrated" spectra $N(E)$, the interpretation of line shapes is much easier and clearer, in particular if one is interested in the information contained in the shape of a spectrum. Publication of experimental integrated spectra $N(E)$ will hopefully become more customary in the future.

The $L_3M_{2,3}V$ spectra of TiN_x, where x varies from 0.5 to 1, are shown in Fig. 7. Again there are two peaks, but separated by approximately 4 eV. The DOS of Ti in TiN_x is rather similar to the corresponding DOS in TiC_x except that the high-energy t_{2g} band lies already below E_F at stoichiometric composition whereas the high-energy e_g band remains above. As a consequence, the high-energy peak in the spectrum of $TiN_{1.0}$ originates fully from the t_{2g}-type PDOS, while the lower one, similar to that of Ti-C, is of slightly more e_g character than t_{2g} character (Fig. 8, bottom right). Reducing the nitrogen concentration leads to a relative decrease of the left peak and an increase of the e_g-like contribution (Fig. 8, top right) so that in the case of $TiN_{0.5}$ the composition of the spectrum is similar to that of $TiC_{0.5}$. No suitable experimental data have been found for a comparison in the case of Ti-N.

As far as Ti-O is concerned, an ordered structure and a partially disordered structure are considered, both referring formally to the stoichiometric composition. The matrix elements used in both calculations were those of the disordered structure with a vacancy concentration of 15% on both sublattices. The result for the partially disordered system is shown in Fig. 9. The shape of the spectrum and the t_{2g} and the e_g contributions are similar to Ti-N except that the energetic separation of the peaks is about 4.6 eV. For ordered Ti-O, the spectrum is rather similar but shows a bigger gap and peak-to-peak ratio. Agreement between theory and experiment is better in the disordered case, as can be seen in Fig. 10 where the experimental data are taken from Solomon and Baun.[16]

IV. SUMMARY

The method to calculate CCV Auger spectra as described in this paper seems to be quite suitable to interpret satisfactorily experimental spectra in terms of energy band-structure-related quantities. For Ti-C and Ti-O it turns out that although the experimental curves are generally broader than those predicted by theory, good agreement is found especially as far as the influence of nonstoichiometry is concerned.

ACKNOWLEDGMENTS

We would like to thank P. Herzig for providing us with the DOS of ordered Ti-O. We also would like to acknowledge a grant by the Austrian Science Foundation (P6285C).

*Present address: Department of Physics and Astronomy, Northwestern University, Evanston, Illinois 60201.

[1]D. Chattarji, *The Theory of Auger Transitions* (Academic, London, 1976).
[2]J. S. Faulkner and G. M. Stocks, Phys. Rev. B **21**, 3222 (1980).
[3]J. Redinger, P. Marksteiner, and P. Weinberger, Z. Phys. B **63**, 321 (1986).
[4]E. Antonides, E. C. Janse, and G. A. Sawatzky, Phys. Rev. B **15**, 1699 (1977).
[5]G. A. Sawatzky, Phys. Rev. Lett. **39**, 504 (1977).
[6]G. A. Sawatzky and A. Lenselink, Phys. Rev. B **21**, 1790 (1980).
[7]M. P. Seah and W. A. Dench, Surf. Interf. Anal. **1**, 2 (1979).
[8]H. Tokutaka, K. Nishimori, and H. Hayashi, Surf. Sci. **149**, 349 (1985).
[9]B. M. Duc, C. Jardin, J. P. Gauthier, G. Thollet, and P. Michel, J. Electron Spectrosc. Relat. Phenom. **20**, 213 (1980).
[10]A. Neckel, P. Rastl, R. Eibler, P. Weinberger, and K. Schwarz, J. Phys. C **9**, 579 (1976).
[11]P. Marksteiner, P. Weinberger, A. Neckel, R. Zeller, and P. H. Dederichs, Phys. Rev. B **33**, 812 (1986).
[12]P. Herzig (private communication).
[13]P. Marksteiner, G. Hörmandinger, and P. Weinberger (unpublished).
[14]D. K. G. de Boer, Ph.D. thesis, Groningen, 1983.
[15]G. L. Gutsev and Y. M. Shul'ga, J. Phys. C **17**, 3269 (1984).
[16]J. S. Solomon and W. L. Baun, Surf. Sci. **51**, 228 (1975).